ACCURACY EVALUATION OF MULTI-SOURCE SATELLITE PRECIPITATION DATA ALONG THE SICHUAN-TIBET RAILWAY IN CHINA

MENG, Q. Y.[1,2] – LI, J. J.[1*] – FENG, Y.[3] – JIANG, X. W.[3] – CHEN, B.[2]

[1]*Chengdu University of Information Technology, Chengdu 610000, China*

[2]*Qianxinan Prefecture Meteorological Bureau, Xingyi 562400, China*

[3]*Institute of Tibetan Plateau Meteorological, Chengdu 610000, China*

[*]*Corresponding author*
e-mail: ljj@cuit.edu.cn; phone: +86-135-5138-3013

(Received 5th Nov 2024; accepted 4th Feb 2025)

Abstract. High spatiotemporal resolution (satellite precipitation data: SPD) are vital for railway planning and risk management, as well as advancing research in geoinformation science and meteorology. Four SPD (Climate Prediction Center Morphing technique: CMORPH, Precipitation Estimation from Remotely Sensed Information using Artificial Neural Networks-Climate Data Record: PERSIANN-CDR, Global Precipitation Measurement IMERG's third-level fusion product: GPM-EARLY, GPM-LATE) were compared with ground-based observations along the (Sichuan-Tibet Railway: STR) in China. Through quantitative and categorical evaluations across different temporal scales, and validation using extreme precipitation indices, the study finds that GPM generally outperforms other datasets, though PERSIANN-CDR exhibits the largest errors. The SPD show the highest correlation on the monthly scale, with significant variability at the annual scale. Errors in PERSIANN-CDR and CMORPH increase with rising monthly precipitation, peaking in July, while GPM demonstrates greater stability. Although PERSIANN-CDR captures precipitation events well, it has a high false alarm rate, whereas GPM-LATE achieves better skill scores. SPD retrieval capabilities decline with increasing precipitation, particularly above 25 mm/day. Spatial analysis shows better data quality in the eastern and southern regions, with GPM performing better. CMORPH accurately captures extreme precipitation indices, followed by PERSIANN-CDR, while GPM tends to overestimate extreme precipitation. These findings are crucial for improving precipitation estimation accuracy and enhancing water resource management and disaster warning systems along the STR.

Keywords: *assessment, comparison, railway engineering, multi-time scale, extreme precipitation indices*

Introduction

Railway construction, essential for national strategy and economic growth, faces significant safety threats from frequent precipitation events, causing thousands of accidents across China over the past 40 years, particularly in the form of flash floods and landslides (Liu et al., 2021). The critical role of the STR in China's transport network and western economic development is underscored by the prevalence of precipitation-induced geological hazards (Li et al., 2019; Liu et al., 2022),which underscores the necessity for accurate precipitation data in railway planning and risk management.

The traditional sources of precipitation data, form meteorological stations and weather radars, are sparse in complex terrains, limiting the acquisition of precision spatiotemporal data. Despite their percison over extensive distances, weather radars are constrained by high costs, signal instability, and constrained coverage. The advent of high-resolution, wide-coverage SPD data has become pivotal for rainfall monitoring and climate change analysis (Sahoo et al., 2011; Liu and Allan, 2012; Yang et al., 2013; Hamada et al., 2015).

http://www.aloki.hu ● ISSN 1589 1623 (Print) ● ISSN 1785 0037 (Online)
DOI: http://dx.doi.org/10.15666/aeer/2303_39874005

However, SPD retrieval, as an indirect method, exhibits notable reliability variations among different sensors and discrepancies from actual measurements (Kidd and Huffman, 2011; Kidd and Levizzani, 2011). In recent years, significant progress has been made in the evaluation and research of SPD (Yang and Luo, 2014; Guo et al., 2016; Sun et al., 2018b; Zhang et al., 2022). Using ground-based precipitation observations as a benchmark, the cetainty and variability of data are assessed and analyzed at various scales. Sun et al. (2018a) comprehensively compared and evaluated 30 global precipitation datasets, revealing significant differences in precision among different products, which are influenced by the number of ground stations, retrieval algorithms, and assimilation models. In Morocco, the GPM series products exhibit high reliability for light to moderate precipitation events (Ait Dhmane et al., 2023). In the Sultanate of Oman, GPM and (Global Satellite Mapping of Precipitation: GSMaP) effectively delineate precipitation patterns, with GSMaP generally outperforming IMERG (Shawky et al., 2019). Evaluation of precipitation products in India highlights the high performance of (Climate Hazards Group InfraRed Precipitation with Station: CHIRPS) and (Tropical Rainfall Measuring Mission Multi-satellite Precipitation Analysis: TMPA) (Prakash, 2019), while in Latin America, different products show varied performance across different basins and temporal scales (Baez-Villanueva et al., 2018). In China, extensive evaluations focusing on the Qinghai-Tibet Plateau indicate that GPM precipitation products exhibit spatiotemporal variability linked to precipitation intensity (He, 2023). Research also suggests that GPM performs better than TRMM in terms of precipitation detection, yet percision in detecting precipitation remains a challenge in high-altitude and harsh climate regions of the Qinghai-Tibet Plateau (Yu et al., 2018). In the Yarlung Tsangpo River Basin, integrated assessments suggest (The China Meteorological Forcing Datase: CMFD) and CMORPH are more suitable for regional hydro-meteorological studies (Ban et al., 2023), while Sun et al. (2020) indicate overall underestimation by GPM and severe overestimation by PERSIANN-CDR. Lin et al. (2022) evaluated six SPD along the STR, most of the SPD were able to effectively capture precipitation features at multiple time scales and identify the best products for different temporal resolutions, and emphasised the importance of accurate precipitation data for meteorological services and disaster prevention in complex terrains, such as the eastern Tibetan Plateau. A multi-satellite product assessment highlights individual strengths and weaknesses, enabling optimal data integration (Levizzani et al., 2020). Precipitation data across different time scales cater to applications like daily weather and flood warnings, and long-term climate studies. These studies illustrate the diverse evaluations of SPD worldwide, showing varying accuracies and strengths of different products across different regions and temporal scales, each presenting both potential and challenges in their application.

Here, four SPD namely CMORPH, PERSIANN-CDR, GPM-EARLY and GPM-LATE were collected along the STR from 2015 to 2022. By employing both quantitative and categorical assessment metrics, comparing the performance of SPD across various time scales, and analyzing differences of spatial distribution characteristics. The effectiveness of the four SPD in detecting and monitoring high-risk precipitation events is further verified using extreme precipitation indices. While the low spatial resolution of the satellite precipitation data used in this study may not be optimal for precisely tracking the railway path itself. This limitation stems from the general focus on broader regional precipitation patterns rather than specific point-based measurements along the railway line. Nonetheless, the data is valuable for understanding large-scale weather trends and

http://www.aloki.hu ● ISSN 1589 1623 (Print) ● ISSN 1785 0037 (Online)
DOI: http://dx.doi.org/10.15666/aeer/2303_39874005

supporting risk assessments in the broader context of infrastructure planning. Although the low resolution of the data might not capture every localized feature of the railway path, the data provides crucial insights at the regional scale, which is highly relevant for infrastructure projects that involve large areas or extensive planning, such as flood risk management and climate impact assessments. This study primarily aims to offer a regional perspective of precipitation patterns and their extreme events, which can be adapted for broader risk assessments in various infrastructure projects beyond the railway itself. Future studies could explore the integration of multi-resolution datasets, including higher-resolution satellite data and ground-based measurements, to enhance the applicability of the results for specific infrastructure projects.

Materials and methods

Methods

This study evaluates SPD pericision using quantitative, categorical indices, and extreme precipitation indices. Quantitative indices assess overall satellite data accuracy for reliability (Lv and Qi, 2022), while categorical indices confirm the alignment of satellite and ground station precipitation events (Liu et al., 2019). Nearest-neighbor interpolation aligns satellite data with ground station locations. The (inverse distance weighting: IDW) method (Hu et al., 2014) maps the spatial distribution of these indices. Additionally, extreme precipitation indices, which characterize short-duration extreme precipitation and continuous heavy rainfall events, are commonly used to assess the likelihood of regional extreme precipitation occurrences.

Here, five quantitative indicators (Root Mean Square Error: RMSE, Mean Absolute Error: MAE, Nash-Sutcliffe Efficiency Coefficient: NSE, Correlation Coefficient: CC) and Bias were selected. The specific calculation methods are as follows, of which x_i is the i day satellite data. y_i is the precipitation of the meteorological station on the i day, n is the total number of samples:

(1) RMSE epresent the standard deviation of the difference between the satellite and the site, and the value is [0, + ∞). Close to 0 indicates that the errorlessness of the satellite is better.

$$RMSE = \sqrt{\frac{1}{n}\sum_{i=1}^{n}(x_i - y_i)^2} \quad \text{(Eq.1)}$$

(2) MAE present the mean absolute error between the satellite and the station is [0, + ∞), and close to 0 indicates that the errorlessness of the satellite is better.

$$MAE = \frac{1}{n}\sum_{i=1}^{n}|x_i - y_i| \quad \text{(Eq.2)}$$

(3) NSE the value is (- ∞, 1], close to 1 indicating that the satellite data quality is good, close to 0, it indicates that the data quality is close to the average level of the observed value, that is, the overall result is credible; if is far less than 0, then the data is not credible.

$$NSE = 1 - \frac{\sum_{i=1}^{n}(x_i - y_i)^2}{\sum_{i=1}^{n}(y_i - \overline{y})^2} \quad \text{(Eq.3)}$$

http://www.aloki.hu ● ISSN 1589 1623 (Print) ● ISSN 1785 0037 (Online)
DOI: http://dx.doi.org/10.15666/aeer/2303_39874005

(4) CC reflects the degree of linear correlation between the satellite and the site, and the value range is [-1,1]. The closer the absolute value is to 1, the better the correlation is.

$$CC = \frac{\sum_{i=1}^{n}(x_i-\overline{x})(y_i-\overline{y})}{\sqrt{\sum_{i=1}^{n}(x_i-\overline{x})\sum_{i=1}^{n}(y_i-\overline{y})}} \quad \text{(Eq.4)}$$

(5) Bias represents the deviation between the satellite and the station, the value range is (∞, + ∞). BIAS is positive, indicating that the satellite data overestimates the precipitation, and vice versa.

$$Bias = \frac{\sum_{i=1}^{n}(x_i-y_i)}{\sum_{i=1}^{n}y_i} \quad \text{(Eq.5)}$$

This paper employs four categorical metrics (Probability of Detection: POD, False Alarm Rate: FAR, Critical Success Index: CSI, and Brier Skill Score: BSS) (Javanshiri et al., 2021) to assess the satellite's capabilities to capture precipitation events. These metrics are derived from the contingency table of precipitation events (*Table 1*), which corresponds to the consistent detection of precipitation between satellites and ground stations. The extreme precipitation index used in this paper is (Maximum 1-day precipitation: RX1DAY) and (Maximum consecutive 5-day precipitation: RX5DAY).

Table 1. *Tables of surface precipitation events and SPD-captured precipitation events*

		Ground Stations	
		Occurs	**not**
SPD	**Occurs**	hit	false
	not	miss	0

(6) POD represents the proportion of precipitation events correctly identified by the satellite out of the total number of precipitation events, ranging from 0 to 1, with an optimal value of 1.

$$POD = \frac{hit}{hit+miss} \quad \text{(Eq.6)}$$

(7) FAR denotes the proportion of non-precipitation events incorrectly classified as precipitation events by the satellite out of the total number of events detected as precipitation, also ranging from 0 to 1, with an optimal value of 0.

$$FAR = \frac{false}{false+hit} \quad \text{(Eq.7)}$$

(8) CSI takes into account both hit and false alarm rates, reflecting the satellite's ability to accurately monitor actual precipitation events, with a range of 0 to 1, and an optimal value of 1.

$$CSI = \frac{hit}{hit\_miss\_false} \quad \text{(Eq.8)}$$

http://www.aloki.hu ● ISSN 1589 1623 (Print) ● ISSN 1785 0037 (Online)
DOI: http://dx.doi.org/10.15666/aeer/2303_39874005

(9) BSS assigns a value of 1 for the occurrence of an event and 0 for its absence. It integrates reliability, discrimination, and uncertainty, with a range of 0 to 1, and an optimal value of 1.

$$BSS = \frac{1}{n}\sum_{i=1}^{n}(x_i - y_i)^2 \quad \text{(Eq.9)}$$

(10) RX1DAY, RRij be the daily precipitation amount on day i in period j.

$$RX1DAY = \max(RR_{ij}) \quad \text{(Eq.10)}$$

(11) RX5DAY, RR_{kj} be the precipitation amount for the 5-day interval ending k, period j.

$$RX5DAY = \max(RR_{kj}) \quad \text{(Eq.11)}$$

(12) The Inverse Distance Weighting (IDW) interpolation method is a widely used spatial interpolation technique. It assumes that the similarity of attribute values between any two points decreases as the distance increases. Based on this assumption, the interpolated value at a given point is calculated as the weighted average of surrounding known points, where the weights are inversely proportional to the distance. This method heavily relies on the spatial distribution of stations. When the distribution of stations in the study area is uneven, significant interpolation bias often occurs in areas far from stations (Wijemannage et al., 2018).

Data selection and data processing

The daily precipitation data from 64 ground stations (45 regional automatic stations,19 national stations) during 2015-2022 were collected from the Sichuan Meteorological Bureau. Daily data were aggregated into annual and monthly averages, excluding months with more than five missing days. There were too many data gaps during 2020-2022 from regional meteorological station, the analysis period is divided into two periods: 2015-2019 (including 64 stations) and 2015-2022 (including 19 national stations). Detailed information on SPD is shown in *Table 2*.

Table 2. *Information of four kinds of SPD*

SPD	Institutions	Spatial resolution	Time resolution	Download address
CMORPH	NOAA	0.25°	30min	https://www.ncei.noaa.gov/data/
PERSIANN - CDR	UCI	0.25°	1hour	https://chrsdata.eng.uci.edu/
GPM-EARLY	NASA,JAXA	0.1°	30min	https://search.earthdata.nasa.gov/search
GPM-LATE	NASA,JAXA	0.1°	30min	https://search.earthdata.nasa.gov/search

Study area

In China, STR spanning 27-33°N and 90-103°E (*Fig. 1*), linked Sichuan up with Tibet. Total length was about 1838 kilometers, crossing 14 major rivers and 21 peaks over 4000 m. The highest point was at 4400 m, with a total elevation change exceeding 3000 m. It cut through some ecological and sensitive zones of the Qinghai-Tibet Plateau,

http://www.aloki.hu ● ISSN 1589 1623 (Print) ● ISSN 1785 0037 (Online)
DOI: http://dx.doi.org/10.15666/aeer/2303_39874005

such as mountains, high-altitude plateaus, deserts, and areas with frequent severe weather. Characterized by high altitude and variable precipitation, the region poses significant challenges for railway planning and construction. This study aims to identify areas with high precipitation risk by evaluating extreme precipitation indices, which provide important guidance for determining potential risk zones based on rainfall intensity. As climate change intensifies, the frequency and intensity of extreme weather events continue to rise, making extreme precipitation indices a key first step in comprehensive risk assessment. However, it is important to note that extreme precipitation indices are just one of many factors affecting the vulnerability and disaster risk in the region. In addition to precipitation, factors such as topography, soil cover, land use, and soil conditions also play a critical role in determining the intensity of regional risk. These factors, acting together, influence the likelihood of localized disasters such as flooding, landslides, and soil erosion in the area. Therefore, this study only points out the significance of precipitation in one of the steps of risk assessment.

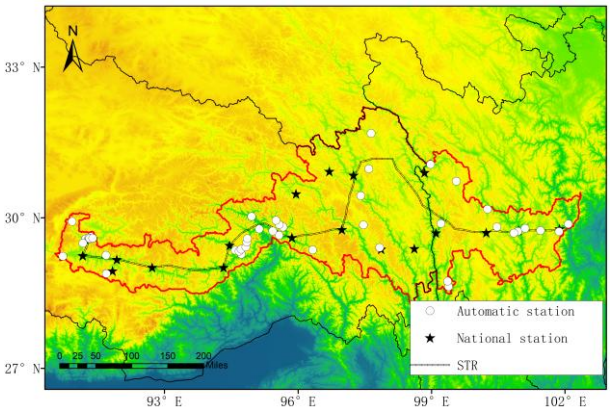

Figure 1. *The locations of STR and meteorological stations*

Results

Quantitative index evaluation at different time scales

The quantitative metrics show a consistent trend with increasing time (*Fig. 2*), with the first stage being overall better than the second. The overall optimization of the GPM, with its small RMSE (*Eq.1*), MAE (*Eq.2*), and NSE (*Eq.3*), suggests a strong stability in terms of accuracy and reproducibility of precipitation estimation, with Bias (*Eq.5*) showing a negative bias (underestimation), while CMORPH and PERSIANN-CDR show positive bias (overestimation). The longer the accumulation period, the greater the difference in error at different time scales. On the daily scale, the bias in 10-day precipitation accumulation becomes more obvious for CMORPH and PERSIANN-CDR. The magnitude of the indicator can reach 60 for monthly scales and more than 400 for annual scales.

The analysis in *Table 3* shows that the CC (*Eq.4*) are higher for shorter time scales (1 day, 3 days, 10 days, and months), indicating that SPD perform better in capturing short-term events. In particular, the performance of PERSIANN-CDR is particularly good on the monthly scale. The performance is weaker on the annual scale, with lower CC values for all SPDs. CMORPH performs well on all time scales, with the best performance on the monthly scale but the weakest performance on the annual scale.

http://www.aloki.hu ● ISSN 1589 1623 (Print) ● ISSN 1785 0037 (Online)
DOI: http://dx.doi.org/10.15666/aeer/2303_39874005

PERSIANN-CDR performs similarly. GPM-EARLY and GPM-LATE perform consistently on shorter time scales, with LATE generally outperforming EARLY, the most important of which is GPM-EARLY and GPM-LATE. where GPM-EARLY is the lowest of all products over the 2015-2022-time scale. In summary, CMORPH and PERSIANN-CDR are more reliable in short- and medium-term precipitation estimation, while GPM is valid in the short- and medium-term, but performs weakly on annual scales.

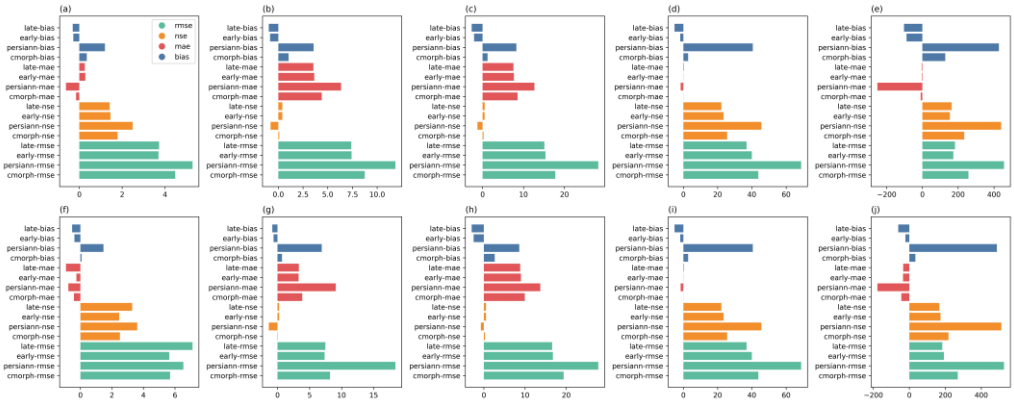

Figure 2. *Distribution of RMSE, MAE, Bias and NSE at day,3-day,10-day, month and year scales:(a-e) 2015-2019, (f-j) 2015-2022*

Table 3. *The absolute value distribution of CC at different time scales*

SPD	Day (20152019)	Day (2015-2022)	3-Day (2015-2019)	3-Day (2015-2022)	10-Day (2015-2019)	10-Day (2015-2022)	Month (2015-2019)	Month (2015-2022)	Year (2015-2019)	Year (2015-2022)
CMORPH	0.61	0.63	0.69	0.71	0.74	0.77	0.84	0.86	0.63	0.48
PERSIANN-CDR	0.51	0.52	0.60	0.59	0.67	0.69	0.87	0.9	0.63	0.47
GPM-EARLY	0.61	0.59	0.69	0.68	0.74	0.79	0.85	0.85	0.65	0.41
GPM-LATE	0.62	0.58	0.70	0.66	0.76	0.80	0.85	0.86	0.68	0.50

Quantitative index evaluation on monthly scale

The monthly index assessments comprehensively evaluate SPD capability to detect and record the nuances of monthly precipitation fluctuations. These assessments are particularly sensitive to the influence of seasonal precipitation patterns and overarching climatic conditions, as referenced in the literature (Shepherd et al., 2014). We can glean profound insights by meticulously examining the repercussions of these monthly precipitation anomalies on the performance of SPD inversion techniques. Such an analysis is pivotal for the rigorous validation and precise calibration of the algorithms at a monthly resolution, thereby ensuring the enhancement and refinement of the quality of satellite-derived precipitation data. The GPM-LATE dataset shows the lowest monthly differences from observed data, following CMORPH (*Fig. 3*). GPM's advantage comes from integrating data from multiple satellites, including the (GPM Core Observatory's: GPMCO) dual-frequency radar, which detects minimal echo intensities Ku-band and employs high-sensitivity interleave sampling Ka-band. The microwave radiometer on GPMCO also bolsters the detection of light and solid precipitation (Tang, 2021). The

http://www.aloki.hu ● ISSN 1589 1623 (Print) ● ISSN 1785 0037 (Online)
DOI: http://dx.doi.org/10.15666/aeer/2303_39874005

LATE version data, further processed from the EARLY version, enhances exactness and reliability (Zhou et al., 2020). All metrics show that errors became larger in the months with more precipitation, especially in the summer. Notably, PERSIANN-CDR and CMORPH errors peak in July, coinciding with the observed maximum monthly precipitation along the railway (data not shown). GPM datasets exhibit a more stable inversion performance during months with significant rainfall, with less pronounced error range increases. Conversely, spring and autumn show an opposite trend, while the winter months, with less precipitation, maintain more consistent performance. Bias (*Eq.5*) analysis indicates that GPM datasets consistently underestimate precipitation from March to October, with the greatest underestimation in September. In contrast, the other data generally overestimate precipitation, with the highest overestimation in July, highlighting the need to reduce CMORPH and PERSIANN-CDR's seasonal sensitivity. A comparison of the two periods reveal slightly smaller errors in the second, with minimal differences noted. SPD inversion effectively captures precipitation information along the entire railway corridor.

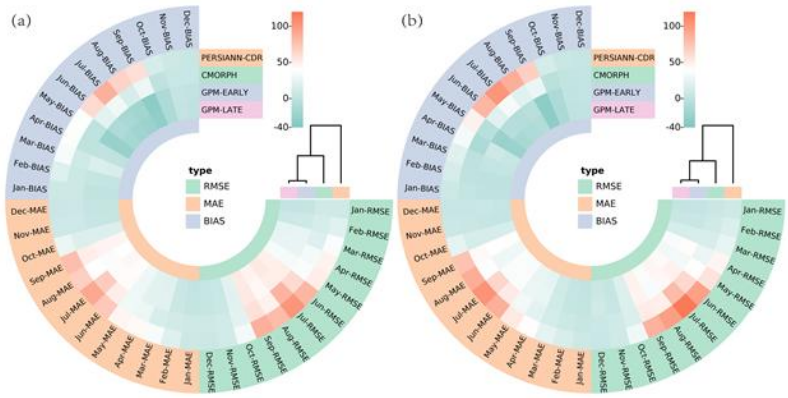

Figure 3. *RMSE, MAE, BIAS monthly distribution: (a) 2015-2019, (b)2015-2022*

The CC monthly distribution (*Fig. 4*) shows higher correlations in wetter months, peaking around 0.8 in August and then declining in September. CC remains relatively consistent for spring, autumn, and winter, ranging from 0.4 to 0.6. CMORPH maintains a stable performance in the first phase, with CC above 0.5, but experiences a significant decrease in the second phase, especially from November to May (CC as low as 0.16 in November). PERSIANN-CDR features are similar to CMORPH, but it shows a high correlation in April and its stability needs to be improved further. GPM data exhibits little monthly variations, though correlations dip in the second period. With a less sample size, individual station variability notably affects overall results, indicating that poor inversion at certain sites can lower overall CC.

Evaluation of daily scale classification index

Categorical evaluation indices are essential for identifying uncertainties in satellite precipitation data (SPD) and for distinguishing correct forecasts from false and missed events. As the time scale increases, the POD (*Eq. 6*) increases significantly, ranging from 0.74 to 0.99, and the FAR (*Eq. 7*) decreases significantly, ranging from 0.16 to 0.58. In particular, the PERSIANN-CDR, which shows a strong ability to capture most of the

http://www.aloki.hu ● ISSN 1589 1623 (Print) ● ISSN 1785 0037 (Online)
DOI: http://dx.doi.org/10.15666/aeer/2303_39874005

precipitation events along the railroad line, with POD values ranging from 0.85 to 0.91, utilizes the Geostationary Orbit infrared imagery from GEO satellites to infer precipitation based on cloud top temperatures, which can lead to a large number of false alarms, as evidenced by the FAR (*Eq. 7*), which ranges from 0.25 to 0.58. The GPM has the lowest false alarm rate, where EARLY has a slightly lower false alarm rate than LATE.

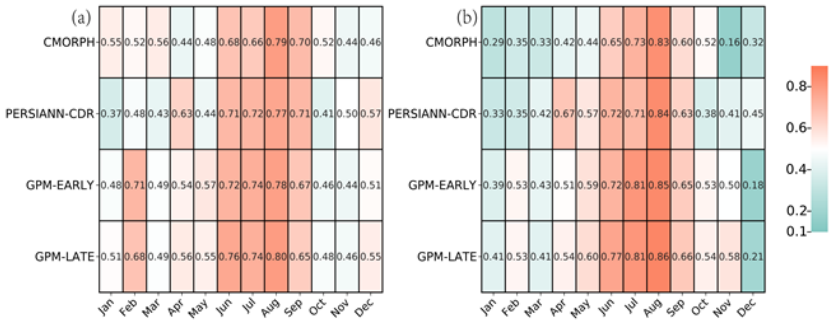

Figure 4. *Monthly correlation coefficient absolute value distribution: (a) 2015-2019, (b)2015-2022*

For CSI (*Eq. 8*) and BSS (*Eq. 9*), we observe different trends on different time scales. BSS takes into account both false alarms and missed events and provides an overall assessment of precipitation forecasting skill. Despite occasional false alarms, GPM typically has fewer false alarms, especially at the 3- and 10-day scales. CMORPH consistently performs at an intermediate level in capturing precipitation events, and BSS also performs at an intermediate level, but lags behind GPM in terms of overall skill. Overall, GPM demonstrates superior skill in both capturing precipitation events and reducing errors at both the 3- and 10-day scales. This makes it the most reliable satellite product for short- and medium-term precipitation forecasting, despite occasional false alarms (*Figure 5*).

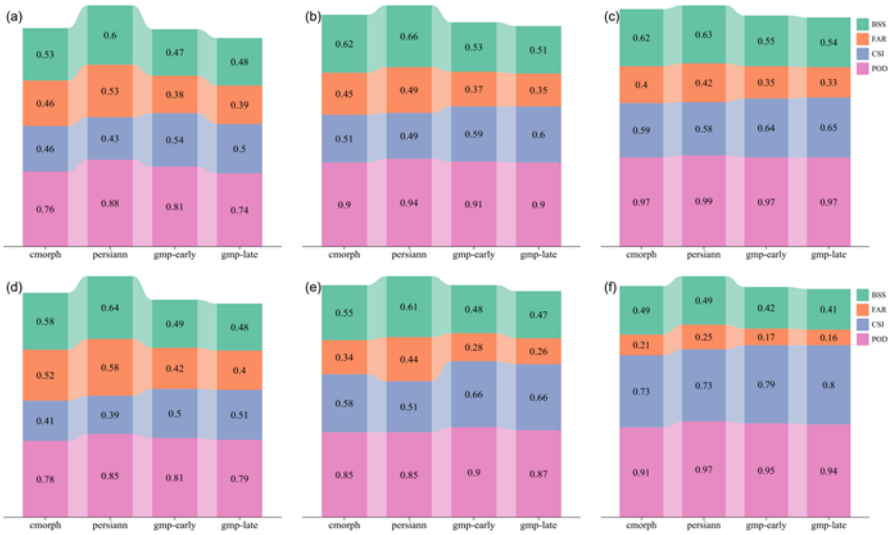

Figure 5. *The evaluation indexes of POD, CSI, FAR and BSS at the day,3-day,10-day scale: (a-c) 2015-2019, (d-f) 2015-2022*

http://www.aloki.hu ● ISSN 1589 1623 (Print) ● ISSN 1785 0037 (Online)
DOI: http://dx.doi.org/10.15666/aeer/2303_39874005

The occurrence of geological disasters is closely related to accumulated precipitation (Lin et al., 2021). In this study, we evaluate categorical indices for five precipitation intensity thresholds: light rain (0.1-4.9 mm), moderate rain (5-9.9 mm), heavy rain (10-14.9 mm), very heavy rain (15-24.9 mm), and extreme precipitation (>25 mm). Results from both periods show consistent patterns (*Fig. 6*), with POD (*Eq. 6*) decreasing sharply as precipitation increases. The POD values for light rain range from 0.3 to 0.63, indicating that the satellites are more effective at detecting precipitation in this threshold. For moderate rain, the POD values range from 0.2 to 0.37, and for heavy rain, the POD is approximately 0.2, reflecting the limited ability of satellites to capture intense precipitation events. This limitation may be due to the infrequency of heavy rainfall along the Sichuan-Tibet Railway and the unique development of convective clouds in plateau areas (Chen et al., 2017). For precipitation greater than 15 mm, the POD gradually increases, with similar patterns observed at the 3-day and 10-day scales. Notably, at the 10-day scale, satellite performance improves due to the cumulative nature of the precipitation event. FAR, CSI, and BSS (*Eq. 7*, *Eq. 8*, and *Eq. 9*) also show that false alarms and missed events increase with higher precipitation intensities. FAR peaks in the heavy rainfall range, while CSI slightly improves for levels above moderate rain, and BSS shows slight improvements in detecting heavy rain as time progresses. For precipitation above 25 mm, the threshold divisions play a role in these metrics, with wider intervals generally reducing false and missed event rates.

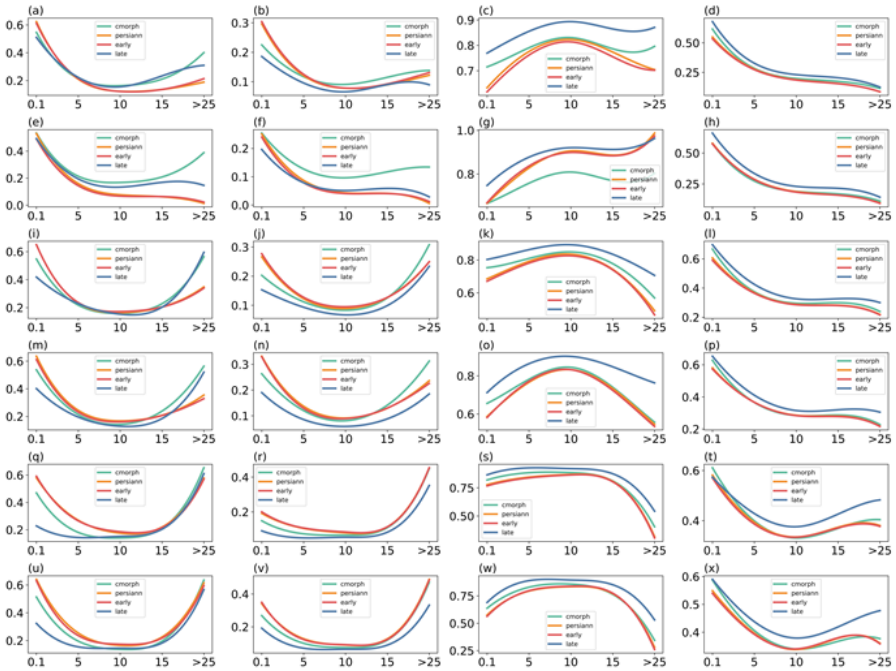

Figure 6. *Categorical metrics (POD, CSI, FAR, BSS) assessed for different precipitation thresholds at daily scales: day (a-d) 2015-2022, (e-h) 2015-2022. 3-day (i-l) 2015-2019, (m-p) 2015-2022. 10-day (q-t): 2015-2022. 2019, (u-x): 2015-2022*

Evaluation results for categorical indices confirm that CMORPH and PERSIANN-CDR achieve higher hit rates, although PERSIANN-CDR exhibits a higher false alarm rate, particularly in the moderate and heavy rainfall categories. On the other hand, GPM excels in detecting light to moderate precipitation, demonstrating superior overall skill in

http://www.aloki.hu ● ISSN 1589 1623 (Print) ● ISSN 1785 0037 (Online)
DOI: http://dx.doi.org/10.15666/aeer/2303_39874005

these categories. For heavy rainfall, CMORPH performs slightly better, which could be attributed to its method of generating motion vectors from multi-satellite infrared (IR) data. This method combines the use of the Special Sensor Microwave/Imager (SSM/I), Advanced Microwave Sounding Unit - B (AMSU-B), and TRMM Microwave Imager (TMI) algorithms, which provide continuous spatial distribution of precipitation and enhance the detection of intense precipitation events (Xie et al., 2017).

The spatial distribution of the two types of indicators on daily scale

Spatial distribution of quantitative indicators at daily scale

Evaluation indices' spatial distribution exposes variations, pinpoints value hotspots and trends, potentially linked to topography, signal interpretation, or station distribution. Recognizing these patterns is key for preemptive risk strategies and resource planning along railway lines. Due to the decreased station count to 19 in the second period, affecting interpolation reliability, this analysis only addresses the spatial characteristics in the first period (2015-2019).

The daily spatial analysis (*Fig. 7*) shows western regions outperform eastern ones in RMSE, but along the Basu-Linzhi section, MAE and RMSE trends diverge, emphasizing the need for a multi-faceted error analysis due to satellite retrieval discrepancies. The data quality along the southern part of the railway is superior to that of the northern part, where a significant high-value area is observed. None of the four types of SPD have been able to accurately infer the precipitation conditions in the northern part of the railway. Bias analysis indicates a consistent underestimation in the Basu-Linzhi section and overestimation elsewhere, except for PERSIANN-CDR, which has a greater tendency to underestimate. The CMORPH data shows a smaller Bias in the central region, which suggests either error cancellation or low inherent errors, making it the best performer there. In correspondence with the distribution of MAE and RMSE, CMORPH also indicates that the central area has lower values, from which it can be concluded that CMORPH performs the best in inferring the central region, followed by GPM. High correlations are seen between Chengdu-Litang and Linzhi-Lasa, while a weak correlation is observed between Baiyu-Bomi. GPM-LATE maintains the closest match to actual conditions.

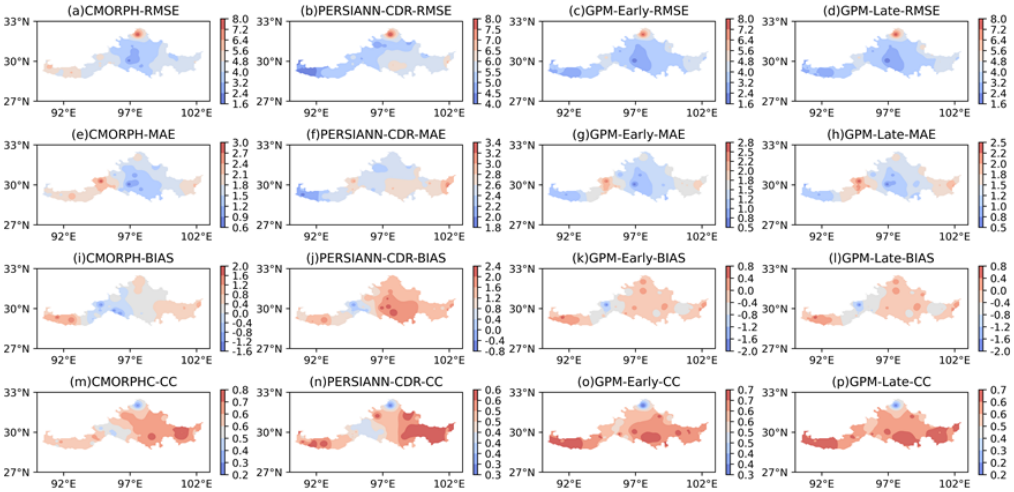

Figure 7. *Spatial distribution of quantitative indicators (a-d) RMSE, (e-f) MAE, (i-l) CC, (m-p) BIAS*

http://www.aloki.hu ● ISSN 1589 1623 (Print) ● ISSN 1785 0037 (Online)
DOI: http://dx.doi.org/10.15666/aeer/2303_39874005

Spatial distribution of classification index on daily scale

Analyzing categorical indicators (*Fig. 8*), CMORPH shows better performance in the Chengdu-Kangding segment, while the other three products perform worse in the Basu-Linzhi segment, though with lower FAR. High FAR values are mainly concentrated in the eastern region, where performance is generally better. Thus, all datasets should be considered for optimal railway precipitation event prediction. Using CSI and BSS to assess reliability, detail, and uncertainty, results are consistent. CSI reveals lower scores for CMORPH and PERSIANN in the central to southern areas, with GPM outperforming with greater consistency. BSS indicates poorer scores for the middle to later railway sections (Gongbujiangda-Bomi), which improve later on.

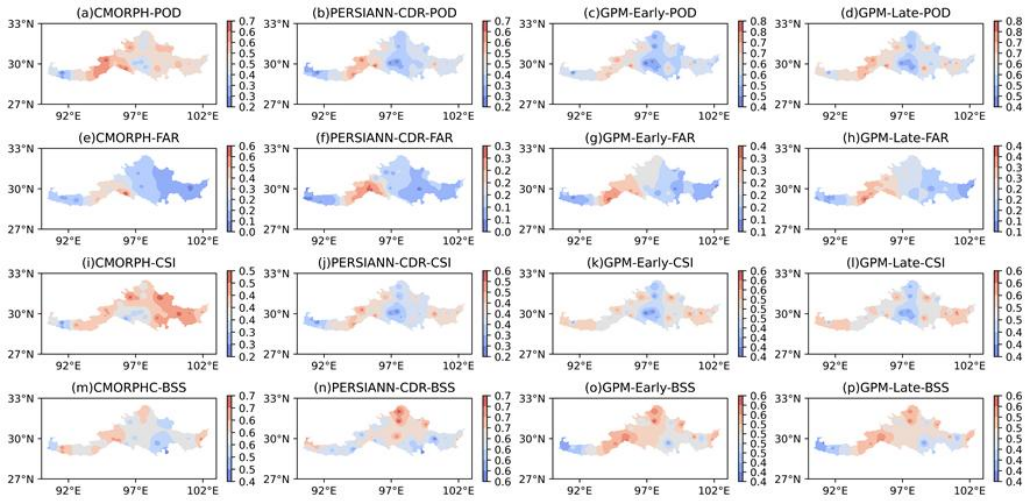

Figure 8. *Spatial distribution of classification indices (a-d) POD, (e-f) FAR, (i-l) CSI, (m-p) BSS*

Summarily, SPD quality excels in the east and south. Observed retrieval errors on specific sections may be linked to station distribution and terrain altitude, suggesting a need for improved data collection in under-monitored highland regions. GPM shows consistent performance with minimal error variation across stations and effective precipitation capture.

Application of extreme precipitation index

Extreme precipitation indices reflect the intensity of precipitation events over short periods and reveal the cumulative effects of precipitation in the short term, which is particularly significant for assessing flood risk. Analyzing these indices allows us to understand the risks and challenges faced by different sections of the STR in dealing with extreme precipitation events. From the spatial distribution of RX1DAY (*Eq.10*) in *Fig. 9*, it can be observed that the actual values predominantly range between 40-80 mm, with a high-value area (>200 mm) in the northern region. Both PERSIANN and CMORPH show magnitudes similar to the actual observations, with similar distribution characteristics; however, they fail to capture the extreme precipitation in the northern part of the railway. CMORPH, in particular, captures extreme precipitation exceeding 100 mm in the western section of the STR. The two GPM products exhibit similar characteristics, with LATE

http://www.aloki.hu ● ISSN 1589 1623 (Print) ● ISSN 1785 0037 (Online)
DOI: http://dx.doi.org/10.15666/aeer/2303_39874005

showing slightly higher magnitudes and a broader extent than EARLY. However, both differ significantly from the actual observations, with exaggerated magnitudes and larger spatial extents.

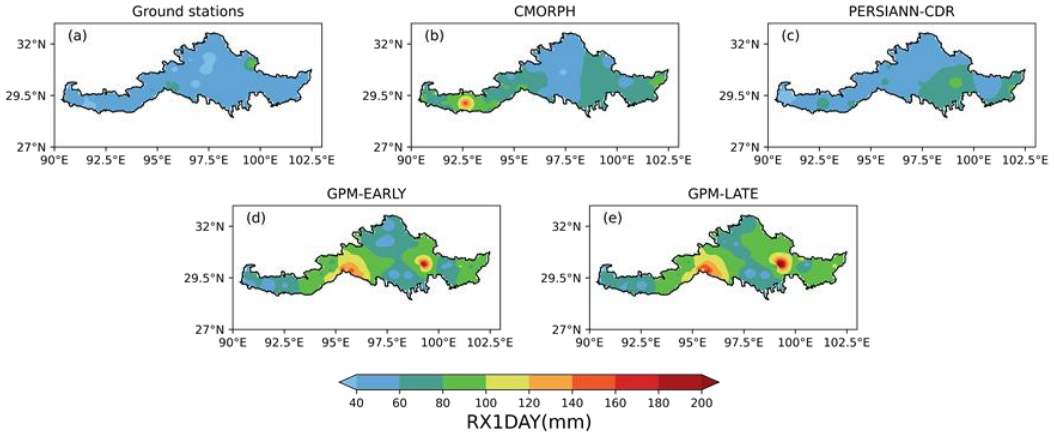

Figure 9. *RX1DAY spatial distribution: (a) Ground stations, (b) CMORPH, (c) PERSIANN-CDR, (d) GPM-EARLY, (e) GPM-LATE*

Analyzing the spatial distribution of RX5DAY (*Eq.11*) in *Fig. 10*, the ground station results indicate values concentrated between 100-160mm, with a high-value area in the northeastern part of the STR, similar to RX1DAY. CMORPH accurately captures the magnitude of this index but overestimates the values in the western section of the STR and fails to correctly capture the high-value area in the north. PERSIANN-CDR overestimates the magnitudes along the central and southern parts, while both GPM products still show stronger results in the western section, with values exceeding 300 mm.

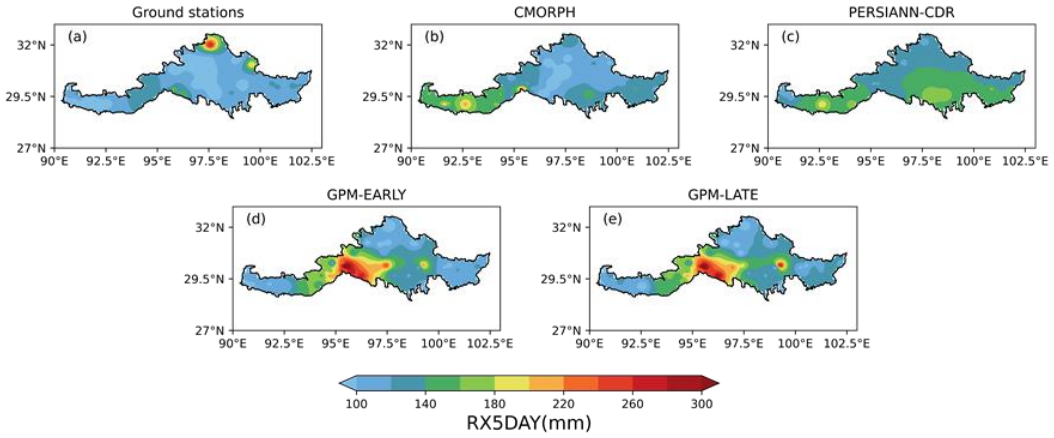

Figure 10. *As the same as Fig. 9, but for the RX5DAY*

After qualitatively analyzing the spatial distribution differences of extreme precipitation indices, we now quantitatively assess the BIAS between SPD and ground station extreme precipitation indices. As shown in *Fig. 11*, all four SPD tend to overestimate the extreme indices, with greater errors in RX1DAY compared to RX5DAY. *Figs. 11(a-d)* indicate that CMORPH is generally reliable, with most

http://www.aloki.hu ● ISSN 1589 1623 (Print) ● ISSN 1785 0037 (Online)
DOI: http://dx.doi.org/10.15666/aeer/2303_39874005

overestimations between 10% and 50%, but with deviations exceeding 100% in the western section of the STR. PERSIANN-CDR results are mostly within 40%, with underestimations primarily in the northern section. GPM performs the worst, with overall overestimations exceeding 70%, particularly in the central section, where BIAS surpasses 100%. The BIAS distribution for RX5DAY in *Fig. 11(e-h)* is similar to RX1DAY, with CMORPH showing the smallest errors, mostly within 30%, while the other three products exhibit errors exceeding 30%, and in the central section, all exceed 70%.

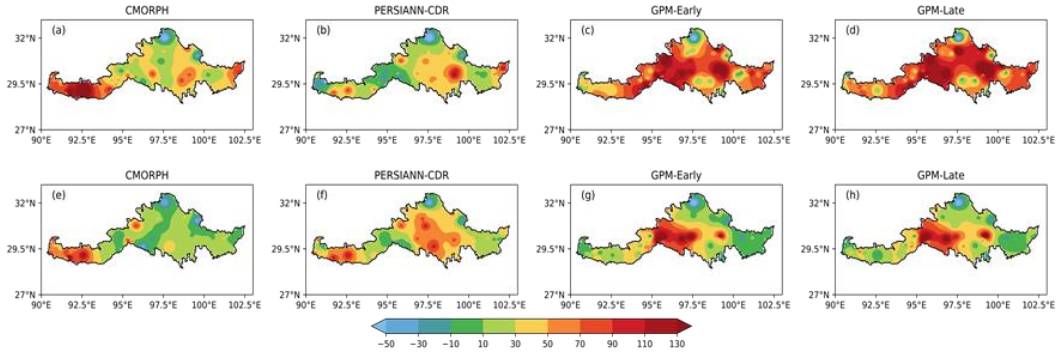

Figure 11. *Spatial distribution of BIAS(%), (a-d) for RX1DAY, (e-h) for RX5DAY*

Summarizing, CMORPH shows lower errors and more precise precipitation simulation along the railway, while GPM overestimates extreme precipitation, exceeding 100% error, cautioning its use in research. PERSIANN-CDR reasonably estimates precipitation but has area discrepancies. The datasets' inability to accurately capture railway precipitation stems from challenging terrain along the STR and IDW's limitations. Terrain interference affects satellite signal accuracy, especially in valleys and ridges, where precipitation may be under-detected. Additionally, weather discontinuity and sparse stations lead to inadequate sampling of variability, potentially smoothing out IDW interpolations and yielding inaccuracies. Each dataset has unique advantages and disadvantages for railway applications, requiring satellite leverage in data-sparse regions with awareness of station coverage limitations.

The conclusions of interpolation by both IDW are consistent with the findings of Baudena et al. (2021) which states that dense station distribution can significantly reduce interpolation errors. However, compared to studies conducted in the eastern margin of the Tibetan Plateau (Xiong et al., 2019), this method tends to overestimate values in high-altitude regions, which may be related to complex terrain, sparse meteorological stations, and the small-scale characteristics of extreme precipitation events. Interpolation of extreme precipitation events often exhibits strong local characteristics because the ability to "spread" the extreme values of a single station is limited, potentially underestimating or overestimating extreme precipitation in surrounding areas (Camera et al., 2014). This is particularly evident in scenarios where rainfall centers are unevenly distributed or exhibit sudden localized characteristics, as the method lacks the capability to accurately capture the dynamic processes of mesoscale convective systems.

http://www.aloki.hu ● ISSN 1589 1623 (Print) ● ISSN 1785 0037 (Online)
DOI: http://dx.doi.org/10.15666/aeer/2303_39874005

Discussion

Different satellites invert different algorithms, and improving the algorithms based on the assessment results is the key to improving the accuracy of satellite precipitation products. The GPM product generally outperforms other satellite datasets, utilizing a satellite combination equipped with the Microwave Imager (GMI) and Dual-Frequency Precipitation Radar (DPR), which allows direct detection of water vapor and precipitation particles within clouds (Hou et al., 2014). Furthermore, the high spatial resolution of microwave sensors gives GPM a distinct advantage in spatial localization (Mahmoud et al., 2019). The PERSIANN-CDR, on the other hand, shows significant overestimation, as it relies on a cloud classification system and estimates precipitation using infrared remote sensing data processed by a neural network algorithm. The infrared sensor's sensitivity to cloud-top temperature often leads to misclassifications in complex weather systems, especially when deep convective clouds and stratiform clouds are mixed, resulting in cold cloud tops being mistakenly identified as areas of heavy precipitation (Hong et al., 2004). CMORPH estimates precipitation using ground station data and satellite infrared observations, applying spatiotemporal interpolation techniques (Habib et al., 2012). It demonstrates good spatiotemporal consistency, especially performing well in the estimation of extreme precipitation.

However, precipitation estimation is not only affected by satellite algorithms and observational accuracy, but also by factors such as topography, soil cover, land use, and soil conditions. Specifically, topography plays a critical role in influencing precipitation along railways, especially in mountainous areas, where terrain undulations can alter precipitation flow and accumulation characteristics. In mountainous and hilly regions, precipitation tends to accumulate through rivers, potentially forming mountain floods or debris flows, thereby increasing the risk of damage to railway infrastructure (Bryndal et al., 2017). Soil cover type is also an important factor affecting soil erosion and runoff during precipitation. Good vegetation cover effectively reduces soil erosion and surface runoff, while areas with loose soil or poor vegetation cover are more prone to flooding and landslides during heavy rainfall, increasing the risk to railway infrastructure (Junger et al., 2022). Changes in land use, such as urbanization and agricultural development, often lead to surface hardening and poor drainage, which can exacerbate the speed of flooding, particularly in low-lying areas along railways. These changes significantly increase the risk of flooding along railways (Te Wierik et al., 2021; Baudena et al., 2021). Additionally, soil physical properties, such as water-holding capacity, permeability, and expansiveness, play an important role in railway stability during extreme precipitation events. In particular, in areas with clay and expansive soils, excessive rainfall can lead to soil swelling or slippage, damaging railway infrastructure (Bordoni et al., 2015; Rasigraf and Wagner, 2022). These factors often interact, creating complex disaster risks. Therefore, in railway planning and construction, it is essential to comprehensively consider the impacts of these factors and adopt effective risk prevention and response measures (Varra et al., 2024).

Conclusions

To determine SPD performance along STR, conduct comparisons with the rain gauge observations at multiple timescales (yearly, monthly, daily, 3-daily, 10-daily). In addition, relating to SPD performance are examined in this study. The main conclusions are as follows.

http://www.aloki.hu ● ISSN 1589 1623 (Print) ● ISSN 1785 0037 (Online)
DOI: http://dx.doi.org/10.15666/aeer/2303_39874005

SPD can capture the spatiotemporal characteristics of multi-time scale precipitation of STR to some extent, which can be used to monitor multi-time scale precipitation and extreme precipitation events along the STR, providing meteorological services for the region. Among the three satellites, GPM performs better at multi-time scales along the STR, showing precipitation underestimation, whereas the other two satellites tend to overestimate. At monthly scales, GPM's retrieval performance is more stable, while PERSIANN-CDR and CMORPH show significant seasonal variability in retrieval. As precipitation intensity increases, satellite retrieval capabilities deteriorate rapidly. PERSIANN-CDR exhibits a high hit rate but also high false alarms for station precipitation. Data quality is better in the eastern than the western part along the STR, and in the southern than the northern part, with GPM showing smaller errors across metrics. CMORPH performs well in capturing extreme precipitation, followed by PERSIANN. The limitations of the evaluation system include the influence of station data distribution on assessment results. Future efforts should focus on strengthening the monitoring of actual precipitation data for more accurate comparisons. Additionally, the highly discontinuous nature of weather systems poses a significant challenge for satellite monitoring of rapidly changing precipitation events within relatively small geographic areas. Future improvements may involve reducing resolution and employing additional metrics to further evaluate SPD product disparities.

Acknowledgements. We would like to thank the anonymous reviewers for their helpful feedback and suggestions, which greatly improved the quality of this manuscript.

Funding. Under the auspices of National Key Research and Development Program of China (No. 2023YFC3007504), open fund of key laboratory of flight techniques and flight safety (No. FZ2020KF04), the Youth Innovation Team of China Meteorological Administration (CMA2023QN16), and the Natural Science Foundation of Sichuan Province (No. 2022NSFSC0215).

REFERENCES

[1] Ait Dhmane, L., Moustadraf, J., Rachdane, M., Saidi, M. E., Benjmel, K., Amraoui, F., Ezzaouini, M. A., Ait Sliman, A., Hadri, A. (2023): Spatiotemporal Assessment and Correction of Gridded Precipitation Products in North Western Morocco. – Atmosphere 14(8): 1239. https://doi.org/10.3390/atmos14081239.

[2] Ashouri, H., Hsu, K., Sorooshian, S., Braithwaite, D. K., Knapp, K. R., Cecil, L. D., Nelson, B. R., Prat, O. (2015): PERSIANN-CDR: Daily Precipitation Climate Data Record from Multisatellite Observations for Hydrological and Climate Studies. – Bull. Am. Meteorol. Soc. 96: 69-83. https://doi.org/10.1175/BAMS-D-13-00068.1.

[3] Baez-Villanueva, O. M., Zambrano-Bigiarini, M., Ribbe, L., Nauditt, A., Giraldo-Osorio, J. D., Thinh, N. X., (2018): Temporal and spatial evaluation of satellite rainfall estimates over different regions in Latin-America. – Atmospheric Res. 213: 34-50. https://doi.org/10.1016/j.atmosres.2018.05.011.

[4] Ban, C., Zuo, D., Xu, Z. et al. (2023): Assessment of accuracy and hydrological modeling effectiveness of multi-source precipitation products in alpine regions-taking the Yarlung Tsangpo River Basin and Lhasa River Basin as examples. – Journal of Soil and Water Conservation 37(02): 159-168+226. DOI:10.13870/j.cnki.stbcxb.2023.02.019. (in Chinese).

[5] Baudena, M., Tuinenburg, O. A., Ferdinand, P. A., Staal, A. (2021): Effects of land-use change in the Amazon on precipitation are likely underestimated. – Glob. Change Biol. 27(21): 5580-5587. https://doi.org/10.1111/gcb.15810.

http://www.aloki.hu ● ISSN 1589 1623 (Print) ● ISSN 1785 0037 (Online)
DOI: http://dx.doi.org/10.15666/aeer/2303_39874005

[6] Bordoni, M., Meisina, C., Valentino, R., Lu, N., Bittelli, M., Chersich, S. (2015): Hydrological factors affecting rainfall-induced shallow landslides: From the field monitoring to a simplified slope stability analysis. – Eng. Geol. 193: 19-37. https://doi.org/10.1016/j.enggeo.2015.04.006.

[7] Bryndal, T., Franczak, P., Kroczak, R., Cabaj, W., Kołodziej, A. (2017): The impact of extreme rainfall and flash floods on the flood risk management process and geomorphological changes in small Carpathian catchments: a case study of the Kasiniczanka river (Outer Carpathians, Poland). – Nat. Hazards 88: 95-120. https://doi.org/10.1007/s11069-017-2858-7.

[8] Camera, C., Bruggeman, A., Hadjinicolaou, P., Pashiardis, S., Lange, M. A. (2014): Evaluation of interpolation techniques for the creation of gridded daily precipitation ($1 \times 1km^2$); Cyprus, 1980–2010. – J. Geophys. Res. Atmospheres 119(2): 693-712. https://doi.org/10.1002/2013JD020611.

[9] Chen, Y., Fu, Y., Xian, T., Pan, X. (2017): Characteristics of cloud cluster over the steep southern slopes of the Himalayas observed by CLOUDSAT. – Int. J. Climatol. 37: 4043-4052. https://doi.org/10.1002/joc.4992.

[10] Guo, H., Chen, S., Bao, A., Behrangi, A., Hong, Y., Ndayisaba, F., Hu, J., Stepanian, P. M. (2016): Early as-sessment of Integrated Multisatellite Retrievals for Global Precipitation Measurement over China. – Atmospheric Res. 176-177: 121-133. https://doi.org/10.1016/j.atmosres.2016.02.020.

[11] Habib, E., Haile, A. T., Tian, Y., Joyce, R. J. (2012): Evaluation of the High-Resolution CMORPH Satellite Rainfall Product Using Dense Rain Gauge Observations and Radar-Based Estimates. – J. Hydrometeorol. 13: 1784-1798. https://doi.org/10.1175/JHM-D-12-017.1.

[12] Hamada, A., Takayabu, Y. N., Liu, C., Zipser, E. J. (2015): Weak linkage between the heaviest rainfall and tallest storms. – Nat. Commun. 6: 6213. https://doi.org/10.1038/ncomms7213.

[13] He, K. (2023): Research on multi-source precipitation data fusion and its application in the Qinghai-Tibet Plateau region. – Xihua University. DOI:10.27411/d.cnki.gscgc.2022.000149. (in Chinese).

[14] Hong, Y., Hsu, K.-L., Sorooshian, S., Gao, X. (2004): Precipitation Estimation from Remotely Sensed Imagery Using an Artificial Neural Network Cloud Classification System. – J. Appl. Meteorol. 43: 1834-1853. https://doi.org/10.1175/JAM2173.1.

[15] Hou, A. Y., Kakar, R. K., Neeck, S., Azarbarzin, A. A., Kummerow, C. D., Kojima, M., Oki, R., Nakamura, K., Iguchi, T. (2014): The Global Precipitation Measurement Mission. – Bull. Am. Meteorol. Soc. 95: 701-722. https://doi.org/10.1175/BAMS-D-13-00164.1.

[16] Hu, Q., Yang, D., Li, Z., Mishra, A. K., Wang, Y., Yang, H. (2014): Multiscale evaluation of six high-resolution satellite monthly rainfall estimates over a humid region in China with dense rain gauges. – Int. J. Remote Sens. 35: 1272-1294. https://doi.org/10.1080/01431161.2013.876118.

[17] Javanshiri, Z., Fathi, M., Mohammadi, S. A. (2021): Comparison of the BMA and EMOS statistical methods for probabilistic quantitative precipitation forecasting. – Meteorol. Appl. 28: e1974. https://doi.org/10.1002/met.1974.

[18] Junger, L., Hohensinner, S., Schroll, K., Wagner, K., Seher, W. (2022): Land Use in Flood-Prone Areas and Its Significance for Flood Risk Management-A Case Study of Alpine Regions in Austria. – Land 11: 392. https://doi.org/10.3390/land11030392.

[19] Kidd, C., Huffman, G. (2011): Global precipitation measurement. – Meteorol. Appl. 18: 334-353. https://doi.org/10.1002/met.284.

[20] Kidd, C., Levizzani, V. (2011): Status of satellite precipitation retrievals. – Hydrol. Earth Syst. Sci. 15: 1109-1116. https://doi.org/10.5194/hess-15-1109-2011.

[21] Levizzani, V., Kidd, C., Kirschbaum, D. B., Kummerow, C. D., Nakamura, K., Turk, F. J. (eds.) (2020): Satellite Precipitation Measurement: Volume 1. – Springer International Publishing.

http://www.aloki.hu ● ISSN 1589 1623 (Print) ● ISSN 1785 0037 (Online)
DOI: http://dx.doi.org/10.15666/aeer/2303_39874005

[22] Li, X., Cui, Y., Zhang, X. et al. (2019): Types, characteristics, and spatial distribution patterns of landslide disasters along the entire Sichuan-Tibet Railway line. – Journal of Engineering Geology 27: 119-129. DOI:10.26914/c.cnkihy.2019.014704. (in Chinese).
[23] Lin, W., Yin, K., Wang, N., Xu, Y., Guo, Z., Li, Y. (2021): Landslide hazard assessment of rainfall-induced landslide based on the CF-SINMAP model: a case study from Wuling Mountain in Hunan Province, China. – Nat. Hazards 106: 679-700. https://doi.org/10.1007/s11069-020-04483-x.
[24] Lin, Z., Yao, X., Du, J., Zhou, Z. (2022): Refined Evaluation of Satellite Precipitation Products against Rain Gauge Observations along the Sichuan-Tibet Railway. – J. Meteorol. Res. 36: 779-797. https://doi.org/10.1007/s13351-022-1226-z.
[25] Liu, C., Allan, R. P. (2012): Multisatellite observed responses of precipitation and its extremes to interannual climate variability. – J. Geophys. Res. Atmospheres 117(D3). https://doi.org/10.1029/2011JD016568.
[26] Liu, J., Xu, Z., Zhao, H. et al. (2019): Evaluation of precipitation inversion accuracy using different satellite data-taking the Yarlung Tsangpo River Basin as an example. – Plateau Meteorology 38(02): 386-396. (in Chinese).
[27] Liu, K., Wang, M., Zhou, T. (2021): Increasing costs to Chinese railway infrastructure by extreme precipitation in a warmer world. – Transp. Res. Part Transp. Environ. 93: 102797. https://doi.org/10.1016/j.trd.2021.102797.
[28] Liu, J., Guo, H., Deng, G. (2022): Study on precipitation thresholds for inducing geological disasters along the Sichuan section of the Sichuan-Tibet Railway. – Journal of Disaster Science: 37(01): 83-91. (in Chinese).
[29] Lv, A., Qi, S. (2022): Applicability assessment of remote sensing and reanalysis precipitation products in da-ta-scarce arid inland basins. – Journal of Geoinformation Science 24(9): 1817-1834. (in Chinese).
[30] Mahmoud, M. T., Hamouda, M. A., Mohamed, M. M. (2019): Spatiotemporal evaluation of the GPM satellite precipitation products over the United Arab Emirates. – Atmospheric Res. 219: 200-212. https://doi.org/10.1016/j.atmosres.2018.12.029.
[31] Prakash, S. (2019): Performance assessment of CHIRPS, MSWEP, SM2RAIN-CCI, and TMPA precipitation products across India. – J. Hydrol. 571: 50-59. https://doi.org/10.1016/j.jhydrol.2019.01.036.
[32] Rasigraf, O., Wagner, D. (2022): Landslides: An emerging model for ecosystem and soil chronosequence research. – Earth-Sci. Rev. 231: 104064. https://doi.org/10.1016/j.earscirev.2022.104064.
[33] Sahoo, A. K., Pan, M., Troy, T. J., Vinukollu, R. K., Sheffield, J., Wood, E. F. (2011): Reconciling the global terrestrial water budget using satellite remote sensing. – Remote Sensing of Environment 115(8): 1850-1865. https://webofscience.clarivate.cn/wos/alldb/full-record/WOS:000292235400006.
[34] Shawky, M., Moussa, A., Hassan, Q. K., El-Sheimy, N. (2019): Performance Assessment of Sub-Daily and Daily Precipitation Estimates Derived from GPM and GSMaP Products over an Arid Environment. – Remote Sens. 11: 2840. https://doi.org/10.3390/rs11232840.
[35] Shepherd, J. M., Grundstein, A. J., Mote, T. L. (2014): An analysis of seasonal biases in satellite and reanalysis rainfall products in the Savannah River basin. – Phys. Geogr. 35.
[36] Sun, Q., Miao, C., Duan, Q., Ashouri, H., Sorooshian, S., Hsu, K. (2018a): A Review of Global Precipitation Data Sets: Data Sources, Estimation, and Intercomparisons. – Rev. Geophys. 56: 79-107. https://doi.org/10.1002/2017RG000574.
[37] Sun, W., Ma, J., Yang, G., Li, W. (2018b): Statistical and Hydrological Evaluations of Multi-Satellite Precipitation Products over Fujiang River Basin in Humid Southeast China. – Remote Sens. 10: 1898. https://doi.org/10.3390/rs10121898.
[38] Sun, H., Su, F. (2020): Evaluation of multiple precipitation datasets and their potential utilities in hydrologic modeling over the Yarlung Zangbo River Basin. – Prog. Geogr. 39: 1126-1139. https://doi.org/10.18306/dlkxjz.2020.07.006.

http://www.aloki.hu ● ISSN 1589 1623 (Print) ● ISSN 1785 0037 (Online)
DOI: http://dx.doi.org/10.15666/aeer/2303_39874005

[39] Tang, G. (2019): Verification, application, and improvement of satellite remote sensing precipitation on a global and regional scale. – Tsinghua University, PhD dissertation. doi:10.27266/d.cnki.gqhau.2019.000409. (in Chinese).
[40] Te Wierik, S. A., Cammeraat, E. L. H., Gupta, J., Artzy-Randrup, Y. A. (2021): Reviewing the Impact of Land Use and Land-Use Change on Moisture Recycling and Precipitation Patterns. – Water Resour. Res. 57(7): e2020WR029234. https://doi.org/10.1029/2020WR029234.
[41] Varra, G., Della Morte, R., Tartaglia, M., Fiduccia, A., Zammuto, A., Agostino, I., Booth, C. A., Quinn, N., Lamond, J. E., Cozzolino, L. (2024): Flood Susceptibility Assessment for Improving the Resilience Capacity of Railway Infrastructure Networks. – Water 16: 2592. https://doi.org/10.3390/w16182592.
[42] Wijemannage, A. L. K., Ranagalage, M., Perera, C. (2018): Comparison of spatial interpolation methods for rainfall data over Sri Lanka. – Conference: Asian Association on Remote Sensing.
[43] Xie, P., Joyce, R., Wu, S., Yoo, S.-H., Yarosh, Y., Sun, F., Lin, R. (2017): Reprocessed, Bias-Corrected CMORPH Global High-Resolution Precipitation Estimates from 1998. – J. Hydrometeorol. 18: 1617-1641. https://doi.org/10.1175/JHM-D-16-0168.1.
[44] Xiong, J., Yong, Z., Wang, Z., Cheng, W., Li, Y., Zhang, H., Ye, C., Yang, Y. (2019): Spatial and Temporal Patterns of the Extreme Precipitation across the Tibetan Plateau (1986–2015). – Water 11: 1453. https://doi.org/10.3390/w11071453.
[45] Yang, J., Gong, P., Fu, R., Zhang, M., Chen, J., Liang, S., Xu, B., Shi, J., Dickinson, R. (2013): The role of satellite remote sensing in climate change studies. – Nat. Clim. Change 3: 875-883. https://doi.org/10.1038/nclimate1908.
[46] Yang, Y., Luo, Y. (2014): Evaluating the performance of remote sensing precipitation products CMORPH, PERSIANN, and TMPA, in the arid region of northwest China. – Theor. Appl. Climatol. 118: 429-445. https://doi.org/10.1007/s00704-013-1072-0.
[47] Yu, K., Zhang, Y., Ma, N. (2018): Applicability assessment of GPM and TRMM remote sensing precipitation products in central Qinghai-Tibet Plateau. – Research of Arid Areas 35(6): 1373-1381. DOI:10.13866/j.azr.2018.06.14. (in Chinese).
[48] Zhang, Y., Wu, C., Yeh, P. J.-F., Li, J., Hu, B. X., Feng, P., Lei, Y. (2022): Evaluation of multi-satellite precip-itation products in estimating precipitation extremes over mainland China at annual, seasonal and monthly scales. – Atmospheric Res. 279: 106387. https://doi.org/10.1016/j.atmosres.2022.106387.
[49] Zhou, Z., Guo, B., Xing, W., Zhou, J., Xu, F., Xu, Y. (2020): Comprehensive evaluation of latest GPM era IMERG and GSMaP precipitation products over mainland China. – Atmospheric Res. 246: 105132. https://doi.org/10.1016/j.atmosres.2020. 105132.

http://www.aloki.hu ● ISSN 1589 1623 (Print) ● ISSN 1785 0037 (Online)
DOI: http://dx.doi.org/10.15666/aeer/2303_39874005